CO/Water and UV−vis Assisted Assembly of Nanostructured Platinum Wires in Mesoporous Silica

Mohamed Mokhtar Mohamed*,† and Mohamed Thabet‡

Chemistry Department, Faculty of Science, Benha University, Benha, Egypt, Chemistry Department, Faculty of Science, Al-Azhar University, Nasr City, Cairo, Egypt

Received: February 2, 2008; Revised Manuscript Received: March 29, 2008

This work describes a method to synthesize free-standing nanoplatinum wires (8−25 nm diameter and 30−100 nm length) fabricated by CO (200 Torr)/water (20 Torr) under a high-pressure Hg lamp at 300 K, for 36 h, induced from H_2PtCl_6 impregnated with FSM-16 (2.7 nm). On the other hand, stabilized platinum nanoparticles (spherical) grown by consecutive reductive carbonylation of a CO (200 Torr) and CO (20 Torr)/water (2 Torr) system at 323 K exhibited mean particle sizes of 2−10 nm. The structure, dispersion behavior, and surface morphology of the materials have been characterized by temperature programmed surface reaction of CO (TPSR), temperature programmed reduction (TPR), N_2 sorpitometry, and transmission electron microscopy techniques. The Pt nanowires showed a higher catalytic activity toward the water−gas shift reaction (WGSR) than that of nanoparticles. It has been shown that the activity does not depend on the structural and morphological characteristics of Pt/FSM-16 such as specific surface area or primary crystallites size but depends on Pt geometry. Investigation of the surface intermediates observed by in situ Fourier transform infrared spectroscopy formed over Pt nanowires and Pt nanoparticles during the WGSR depicted the developing of unidentate formate species on the former and carbonates on the latter. TPSR demonstrated the facile interaction of CO with nanowires (243−373 K) at lower temperatures, presumably dissociatively, than with nanoparticles (243−493 K). The same result was accomplished using TPR, comprehending that complete reduction was attained at 723 K for the former, but it did not reach completion until 873 K for the latter. This indicated that cationic Pt plays a crucial role in catalyzing WGSR at 323 K. Other issues regarding the binding of CO on Pt particles, declining activity with temperatures, and CO cluster bonds either on Pt nanoparticles or nanowires were also discussed.

1. Introduction

Nanometer-scale structures have generated a great deal of interest as potential building blocks for nanostructured materials, composites,[1] nanoscale electronic devices,[1,2] ultrahigh-density magnetic recording systems,[3] and optical devices.[4] Platinum nanoparticles are of particular interest, because they are one of the most stable metal nanoparticles and possess fascinating properties, including their ability to assemble in multiple shapes, and size-related electronic, magnetic, and optical properties, leading to a wide range of applications, including catalysis and biology.[5] Recently, interest in Pt nanorods has increased due to their effectiveness as 1D semiconductors, their efficiency in electron transport, and their potential use in other nanoelectronic devices.[2] Pt should form thinner nanowires than Au,[6] because of the higher nucleation density of Pt islands in an early growth stage and also because of its slower coalescence kinetics. Because of their smaller size, Pt nanowires are expected to have stronger anisotropy than Au nanowires, and they might even show quantum confinement effects due to the limitation of electron movement perpendicular to the nanowire axes.[7] Remarkably, the electrical resistance of the nanowires can change due to chemisorption of species such as hydrogen or amines.[8]

So far, nanowires can be fabricated using many methods, including thermal chemical vapor deposition (CVD), [9] metal-organic CVD,[10] hydrothermal methods,[11] electrochemical deposition,[12–14] sputtering,[15] etc., and great attention has been paid to the continued improvement of these fabrication methods. Although significant advancement has recently been made in fabricating nanowires, they are still far from practical applications. These methods of fabricating nanowires or nanotubes with/without catalysts employ different growth mechanisms. Nonetheless, no method is perfect, and the resulting nanowires still suffer from many artifacts, including imperfections in the characteristics of individual nanowires or nonuniformity among them. Resolving such problems can be assessed through exploiting mesoporous materials that are frequently employed as templates for fabricating nanowires, where arrays of pores inside those materials are filled by an appropriate metal in a liquid state.[16] However, the major problem with this approach is that it is relatively difficult to acquire densely continuous nanowires. Overcoming such problems necessitates injection at high pressure and temperature,[17] which might affect the template itself or the crystalline quality of nanowires. Therefore, a new proposed method to control over the crystalline quality, size, and spacing is very essential.

The application of shape-controlled synthesis of metallic particles in catalysis is relatively new. However, the number of studies using such catalytic systems tends to rapidly increase. Fukuoka et al. reported a direct comparison between catalytic properties of spherical and Pt nanowires synthesized inside a FSM-16 mesoporous template.[18] In the hydrogenolysis of butane, Pt nanowires exhibited a 36 times higher turnover

* To whom correspondence should be addressed. E-mail: mohmok2000@yahoo.com.
† Benha University.
‡ Al-Azhar University.

10.1021/jp8009904 CCC: $40.75
Published on Web 05/21/2008

frequency than spherical particles. Moreover, Pt nanowires were found to produce ethane by secondary−secondary carbon bond cleavage, whereas spherical Pt particles were only able to cleave terminal C−C bonds to produce methane and propane. This change of catalytic properties were ascribed to the preferential exposition of {110} planes and/or to more electron-deficient sites. Therefore, the morphological control during the synthesis of nanoparticles seems to lead to interesting catalytic systems. One cause often advanced to explain these results was related to the preferential exposition of crystallographic planes leading to highly selective catalysts. However, most of the studies were performed using organic ligands[19,20] that can modify catalytic properties by limiting the accessibility of active sites to reactants and intermediates, thus changing catalytic properties.

In view of the structure interests in the mobility and reactivity of Pt carbonyl clusters, we propose for the first time a ship-in-bottle synthesis of Pt wires aligned in the ordered hexagonal channels of FSM-16 (2.7 nm) by templating reduction of Pt salt with CO/water under a high-pressure Hg lamp. The studied reductive carbonylation reaction of H_2PtCl_6 in FSM-16 and the resulting Pt carbonyl clusters of nano-Pt wires were extensively characterized by Fourier transform infrared spectroscopy (FTIR), temperature programmed surface reaction (TPSR), temperature programmed reduction (TPR), N_2 sorptiometry, and transmission electron microscopy (TEM) techniques and compared with the those of nanoparticles (spherical). The structural approach of both Pt wire and particle carbonyl clusters in FSM-16 were studied regarding their interaction with CO, both from diffusion and binding criteria, by measuring the TPSR of CO as well as determining surface intermediates depicted during the reacting CO/water gas mixture by means of in situ FTIR. Their catalytic behavior toward water-gas shift reaction (WGSR) are discussed in conjunction with their coordinative interactions with CO.

2. Experimental

2.1. Sample Preparation. The host FSM-16 of 2.7 nm size was synthesized using a polysilicate (Kanemite; $NaHSi_2O_5 \cdot 3H_2O$) with $C_{16}H_{33}NMe_3Cl$ as a surfactant template according to published procedures.[21] After calcination in air at 823 K, the resulting material ($SiO_2/Al_2O_3 = 320$) presented well-defined hexagonal walls with silanol groups (3745 cm^{-1}) and a characteristic X-ray powder pattern in the low angle region (Cu Kα, $2\theta = 2.30, 4.00, 4.60, 6.10°$).

A sample containing 5 wt% Pt was prepared by impregnation of FSM-16 slurry by slow addition of an aqueous solution of $H_2PtCl_6 \cdot 6H_2O$ with rapid stirring for 1 h. The impregnation was continued for another 12 h at 300 K and then vaccuum-dried (10^{-4} Torr). This sample, which was charged in a quartz cell (15 × 15 × 1.5 mm) and exposed to CO (200 Torr)/water (20 Torr), was irradiated at 300 K by a high-pressure Hg lamp for 36 h [(F18W-BLB) $\lambda > 254$ nm] with a water jacket to avoid external heating. The pale yellow sample gradually turned into pale gray, emphasizing the reduction of $PtCl_6^{2-}$ into metallic Pt wire during irradiation, suggesting that the $PtCl_6^{-2}$ impregnated into mesoporous channels of FSM-16 was reduced.

The Pt nanoparticle sample was also prepared by impregnating FSM-16 with an aqueous solution of H_2PtCl_6 to give 5 wt% Pt loading. The reductive carbonylation was conducted by the exposure of H_2PtCl_6/FSM-16 to 200 Torr of CO followed by a mixture of CO (20 Torr) and H_2O (2.0 Torr) at 323 K. Our goal is to control particle size and shape of platinum nanoparticles using consecutive CO and CO/H_2O mixtures at different times.

2.2. Catalyst Characterization. ***2.2.1. Temperature Programmed Surface Reaction (TPSR).*** The TPSR experiments were performed using an automated gas desorption analyzer (Quadrasorb SI-MP). The sample (50 mg) was loaded in a U-shaped quartz micro reactor and heated from 25 to 50 °C (heating rate, 2 °C/min) in flowing helium (20 mL/min). The sample was then subjected to a CO/He flowing mixture (15 mL/min, 2.48% CO in He); the CO consumption and CO_2 evolution were monitored using a thermal conductivity detector. The TPSR experiments were accomplished following CO adsorption at low temperatures (LTR) as well as at high temperatures (HTR). The adsorption of CO was performed at −40 °C (using a liquid nitrogen trap) followed by increasing the temperature linearly to 400 °C at a ramping rate of 2 °C/min. To monitor the amount of CO_2 evolved and the temperature at which CO_2 occurred apart from those of CO, a dry ice/acetone trap was used.

2.2.2. Temperature Programmed Reduction (TPR). TPR experiments were performed using the same apparatus. After heating the sample at 323 K for 1 h, the H_2/Ar mixture (15 mL/min, 9.98% H_2 in Ar) was introduce to the the sample and was followed by linearly increasing the temperature to 873 K at a constant rate of 2 K/min. These experiments were performed using a dry ice/acetone trap to prevent any interference peaks.

2.2.3. In-situ FTIR. In situ FTIR spectra of the samples were carried out in a closed circulation system with a dead volume of 168 cm^3. An IR cell equipped with NaCl windows was used for pretreatment and measurements. A self-supported wafer (20 mg) was prepared under nitrogen atmosphere and mounted to the sample holder in the IR cell . The wafer was evacuated at the desired temperature for 30 min before adsorption at room temperature. The IR spectra were recorded with a resolution of 2 cm^{-1} using a Jasco double beam FTIR-40.

2.2.4. Transmission Electron Microscope (TEM). TEM micrographs were measured using a Philips, model Tecani Feil2, at an accelerating voltage of 200 KV. The powder samples were put on carbon foil with a microgrid. TEM images were observed with minimum electron irradiation to prevent damage to the sample structure.

2.2.5. Adsorption Measurements. An automated gas sorption analyzer Quantachrome (Quadrasorb SI-MP) instrument was used to measure adsorption and desorption isotherms, surface area, and pore size distribution. The dispersion of platinum inside the FSM-16 sample was measured using CO chemisorption at room temperature under the assumption that $CO/Pt_s = 1.0$ at the monolayer formation. Prior to the measurements, the samples were outgassed to remove physisorbed molecules from the surface (and pores) of the sample (10^{-5} Torr, H_2 reduction at 573 K, for 1 h). To ensure accurate data, the corrected dry sample weight was listed into the data set after the run was finished. This instrument provides a programmable facility to allow the furnace to be computer controlled during the sample preparation and chemisorption data.

2.2.6. Catalytic Reaction. The catalytic performances in the WGSR were studied using a closed circulation system with a Pyrex-glass U-type reactor, which was charged with 100 mg of catalysts. The WGSR proceeded at 323 K and 60 Torr for CO and at 5 Torr for H_2O.[22] The catalysts were treated by heating the samples under vacuum (10^{-4} Torr) at 323 K for 0.5 h prior to the admission of the reacting gas mixture. The gas phase reactants and products were analyzed by on-line gas chromatography (Shimadzu-14C), using Porapak q and molecular sieve 13X, with a thermal conductivity detector operated at 60 °C for the separation of CO, CO_2, and H_2.

Figure 1. TEM image of Pt-nanowires obtained following exposure of a CO/water (200/20 Torr) mixture and a Hg lamp at 300 K.

TABLE 1: Surface Characteristics of Parent and Pt Nanowires and Nanoparticles Encapsulated in FSM-16

sample	surface area (m^2/g)	pore diameter (nm)	dispersion (%)	metal surface area (m^2/g)	reduction temperature (K)
FSM-16	1015	2.93			
5 wt% Pt particles/ FSM-16	750	2.896	7.73	19.1	573
5 wt% Pt wires/FSM-16	827	2.850	8.70	20.2	573

3. Results and Discussion

3.1. Adsorption Measurements and TEM Micrographs. As presented in Figure 1, the TEM image showed that nanostructured Pt wires [8−25 nm diameter and 30−100 nm length] were formed in alignment along the channels of the FSM-16 (2.7 nm) host. Lattice fringes were observed in Pt wires, corresponding to the (110) plane of cubic symmetry of Pt crystals.[23] The electron diffraction pattern implies that Pt wires are single crystals and are arranged in a linear form. The large diameter of the nanowire structure could lead to its coincidence with the cylindrical mesoporous channels of FSM-16; consequently, a significant loss in surface area was expected. However, Table 1 showed that the decrease in surface area for the Pt wire sample is not large (18.5%). This indicates that the wires were not extended throughout the pore diameter of the host FSM-16 (Table 1) but were mostly deep inside the pore volume. The presence of very small amounts of nanoparticles in this image, specifically in the upper part and lower part, evidence that the formation of wires was originally resulted from nanoparticles.

TEM results presented in Figure 2, panels a−c, showed that Pt particles of average diameter of 2−8 nm were formed inside FSM-16. These atoms were uniformly distributed along the ordered mesoporous channels of FSM-16 crystals, that is, they are not prone to aggregation, with significant formation of external particles. The size of nanoparticles that has been tuned in a very narrow margin is typically dependent on the concentration and choice of treatment by the CO and CO/water systems. When the reaction of CO lasted for 8 h at 323 K (Figure 2d), the as-produced nanoparticles became a little larger, with average particles size of 4−10 nm. The Pt dispersion calculated from the CO adsorption, which relates the ratio of the number of surface atoms to the total number of metal atoms, was similar for both wires and particles materials. This advocates the difficulty of determining Pt dispersion using chemisorption methods because of complexity of reaching all active surfaces. Furthermore, both Pt wires and Pt particles maintained very comparable metal surface areas of 17.5 and 19.1 m^2/g, respectively. It seems that the dispersion percentage and the metal surface area values depend on the treatment temperature.

3.2. Temperature Programmed Surface Reaction (TPSR). TPSR of Pt particles/FSM-16 and Pt wires/FSM-16 samples (Figure 3) was carried out, under a flow of 2.48% CO in He, to methodically determine the consumption of CO as well as the formation of CO_2. Figure 3 shows that the up-taken amount of CO in the case of Pt wires in low (LTR) and high temperatures regions (HTR) exceeds those of the Pt particles. This was confirmed through a pair of runs shown while using a N_2 trap (solid line) and dry ice acetone trap (dotted line). These runs had shown that LTR displayed a TPSR peak at −30 °C for both samples, representing the consumption of CO that is frequently expressed in micromoles per mole of metal atoms, CO/Pt. Pt wire indicates that the up-taken amount of CO measures 32 μmol, exceeding that of Pt particles, which was 24 μ mol. The CO/Pt ratios indicate, respectively, 2.5 and 1.9 for Pt wires and Pt particles samples. In LTR, the evolved CO_2 peak that was observed as an upward climax exhibited larger value on wires (7.8 μmol) than on particles (2.5 μmol), suggesting that CO is dissociatively chemisorbed rather than associatively on Pt surfaces[24] substantiated by evoking CO_2 as a desorption peak. This was very largely apparent on nanowires rather than on nanoparticles, revealing the presence of more cationic Pt on the former than on the latter. Assignments of the LTR peaks to the FSM-16 substrate are denied based on earlier studies confirmed from IR spectra of CO interaction with SiO_2[25] that indicate that the H-bonded complex is only formed at liquid N_2 temperature. Consequently, the assignments of this peak to the presence of different Pt states are likely since the interaction probability between Pt and FSM-16 at such low temperatures is very weak. The CO adsorption at LTR indicates the presence of higher binding sites on the wires than those on particles. This could be associated with the change in wires morphology, that is, nanowires own specific geometric constructions of promising atomic arrangements. LTR manifests the reduction feasibility of some of Pt cations at such low temperatures.

In the HTR, the up-taken amount of CO on Pt wires was 22.6 μmol at 100 °C (N_2 trap), and that for Pt particles was 5.7 μmol at 220 °C. The ratio of 1.8 for Pt wires compared with 0.45 for Pt particles indicates that the interaction of the former with CO is markedly favored over that with the latter. This reactivity is emphasized from the possibility of reacting the wires at lower temperature with CO (100 °C) than with the particles (220 °C). This simply means that the activity for CO declines on Pt particles, that is, active sites are comparatively low. An increased amount of CO_2 is evolved at 235 °C on Pt particles in the HTR (dry ice acetone trap), whereas a small amount is noticed on wires, indicating an increase in nanoparticles fraction

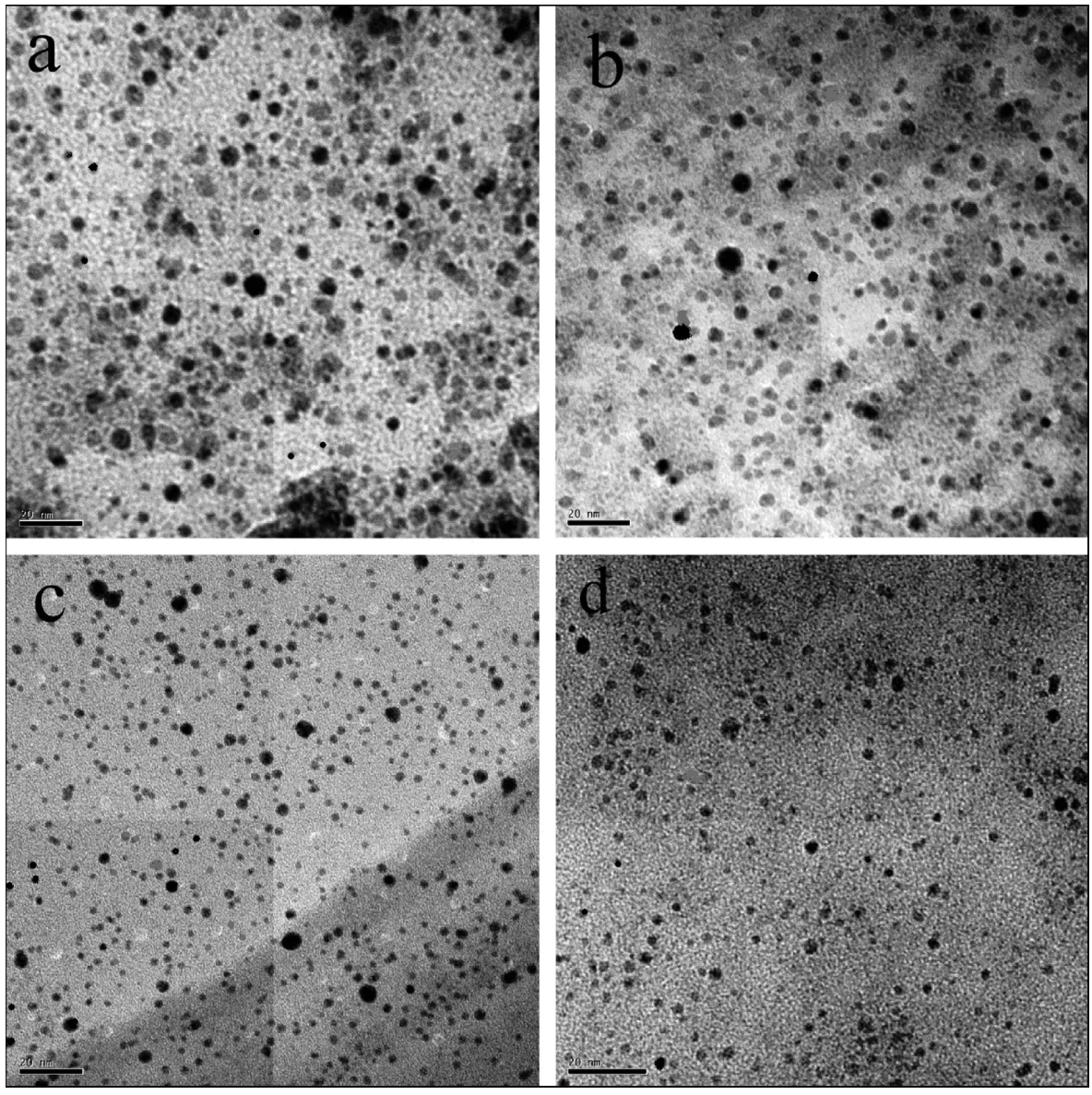

Figure 2. TEM images of Pt nanoparticles obtained at 323 K (a) after exposure to CO (200 Torr, 1 h) and followed by CO/water (20/2 Torr, 1 h); (b) CO (200 Torr, 3 h) followed by CO/water (20/2 Torr, 1 h); (c) CO (200 Torr, 5 h) followed by CO/water (20/2 Torr, 1 h); and (d) CO (200 Torr, 8 h) followed by CO/water (20/2 Torr, 1 h).

reduced. The expected increase following treatment beyond 50 °C is due to increased water vapor accumulations that are eligible to interact with CO and to perform WGS, resulting in more reduced Pt moieties. In Figure 3, the HTR shows significant differences concerning peak broadness and low CO consumption compared with the LTR, emphasizing that great amounts of CO are consumed to build up different carbonyl species (clusters). Undoubtedly, these results demonstrate that cationic Pt usually plays a crucial role in catalyzing CO oxidation either at low temperatures (on nanowires) or at higher ones (on nanoparticles).

3.3. Temperature Programmed Reduction (TPR). TPR profiles of Pt wires and Pt particles encapsulated inside FSM-16 are displayed in Figure 4. The first useful information that TPR provides is the temperatures needed for complete reduction of a material. The TPR pattern of Pt wires/FSM-16 exhibited four peaks, whereas the particles displayed two peaks. The former peaks were maximized at 398, 423, 603, and 723 K, whereas the latter were at 633 and 823 K. A quantitative estimation of the ratios of total hydrogen consumption in units of moles per metal atoms (H_2/Pt), indicates a value of 5 for the overlapped peaks at 398 and 423 K, and 0.50 and 0.50 for 603 and 723 K, respectively. Contrarily, the H_2/Pt ratios on Pt particles measured a lower value of 1.5. The summation of the H_2 consumption related to complete reduction of different oxidized Pt species measured a value of 6.0 on wires and 1.5 on the particles. The value of 6 found for the wire sample is indeed equal to the stoichiometric reduction of the Pt^{6+} salt. This assumes that the FSM-16 substrate did not consume H_2. One can presume that the morphological differences between wires and particles seriously affects the extent of forming Pt metal in both samples in the sense that a complete reduction of the former was accomplished at lower temperatures (723 K) than that required for the latter (823 K). The facile reduction of Pt nanowires compared to nanoparticles affirms that the latter are bound more strongly to the support than the former.

3.4. In-situ FTIR Spectra. ***3.4.1. Pt wire/FSM-16 Sample.*** Figure 5 shows IR spectra of the adsorbed CO/H_2O mixture (P_{CO} = 60 Torr and P_{H_2O} = 5 Torr) on 5 wt% Pt wires/FSM-16, at 323 K, as a function of time. The obtained spectra were

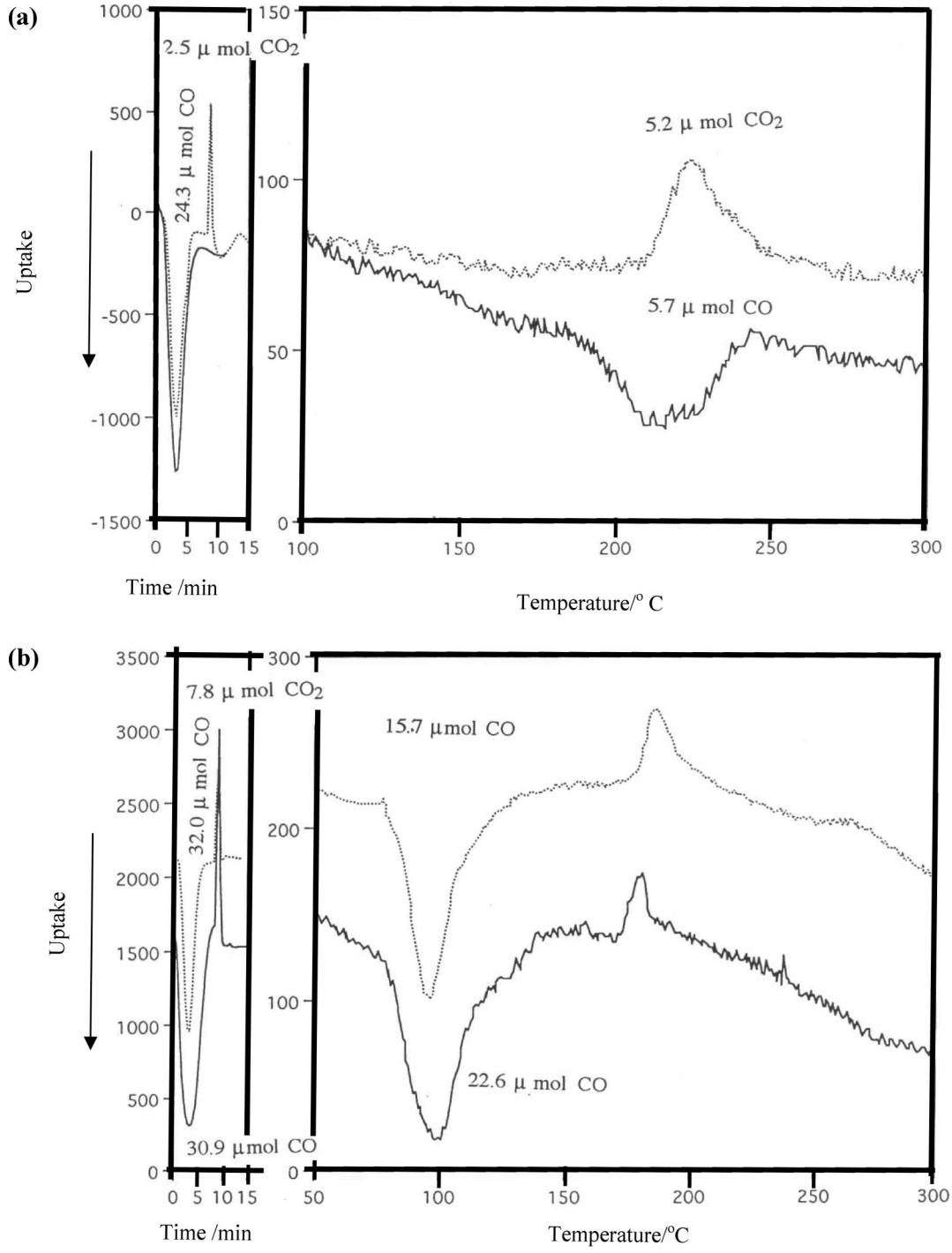

Figure 3. (a) TPSR of CO on Pt nanoparticles while using a liquid N_2 trap (solid line) and dry ice acetone trap (dotted line). (b) TPSR of CO on Pt nanowires (ramping rate = 2 °C/ min, 50 mg sample).

subtracted from background for each spectrum. Trace a shows the bands recorded after admission of the reacting gas mixture for 3 min. Bands at 2188, 2149, 2128_{sh}, 1700, 1628, and 1370 cm^{-1} are detected. From the analogy of the previously reported Pt carbonyl species, the IR bands at 2188, 2149, and 2128 cm^{-1} can be ascribed to *cis*-$Pt(CO)_2Cl_2$ (2188 and 2148 cm^{-1})[26] and $Pt(CO)Cl_3$ (2121 cm^{-1}).[27] These three bands showed a dramatic change in intensity with prolonging the CO/H_2O exposure time. The 2128 cm^{-1} band showed a shift to lower wavenumbers (2105 cm^{-1}) and an increase in intensity at the expense of decreasing the 2188 and 2149 cm^{-1} bands. The latter bands appeared as shoulders as time elapsed. These Pt carbonyls exhibited, after 50 min, a steady-state spectrum (e) of carbonyl bands ($\nu CO = 2096_s$ and 1894_m cm^{-1}). The strong band at 2096 cm^{-1} is typical for metallic Pt on which CO favors the single-atom position due to the relatively large d-band width[28] (valence d-electron orbitals are more extended and, therefore, their interaction with CO would increase). More interestingly, another broad band at 1830 cm^{-1} appeared, indicative of the presence of another bridge-bonded CO. Spectral features analogous to the bands found at 2096 and 1894 cm^{-1} were observed[19] while studying Pt/FSM-16 system exposed to CO (200 Torr) in the temperature range 300−323 K. Accordingly, they attributed these bands to the formation of $[Pt_{15}(CO)_{30}]^{2-}$cluster inside FSM-16 channels. The facile elimination of these bands upon evacuation was displayed by the authors (10^{-4} Torr, 300−323

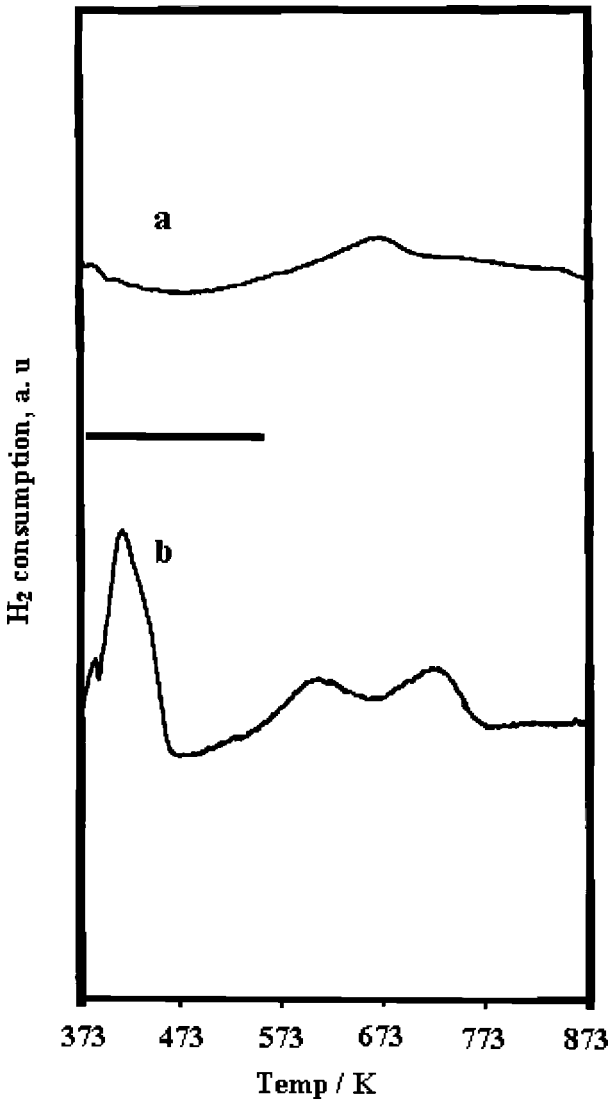

Figure 4. TPR profiles of Pt nanoparticles (a) and Pt nanowires (b) encapsulated in FSM-16.

K). However, in this work relatively stable carbonyl clusters were obtained, even following evacuation at 323 K (10^{-5} Torr). This can be attributed to the stabilizing effect offered by FSM-16 toward the morphological construction of Pt wires prepared by the action of CO/H_2O. The appearance of the bridged 1830 cm^{-1} band suggests the presence of another kind of clusters but of lower concentration.

On the other hand, monitoring the bands in the 1350−1750 cm^{-1} region could give a hint on the intermediates formed on the wire surface, giving a clue on the interaction mechanism. Bands at 1700 and 1370 cm^{-1} can be assigned to unstable carboxylato [C═O (OH)] (νCO 1716 cm^{-1}, νO−C 1370 cm^{-1})[29] or monodentate formate species [O (C═O) similar to those in $C(HgOCOH)_4$ and $Cd(HCOO)_2$ (νC═O 1667−1700 cm^{-1}, νO−C 1337−1360 cm^{-1})].[30] The two bands became more prominent after evacuation at 323 K, whereas the water band at 1628 cm^{-1} is vanished. Because the formation of formate species necessitates another asymmetric band around 1600 cm^{-1}, which could be masked by the deformation band of water, a D_2O is used instead of H_2O in the reacting mixture to indicate the presence of a band at 1620 cm^{-1} (not shown). This result undoubtedly led us to assign the 1370, 1620, and 1700 cm^{-1} bands to formate species, that is, $\nu(OCO)_{as}$, 1620; $\nu(OCO)_s$, 1370; and νC═O, 1700 cm^{-1}.

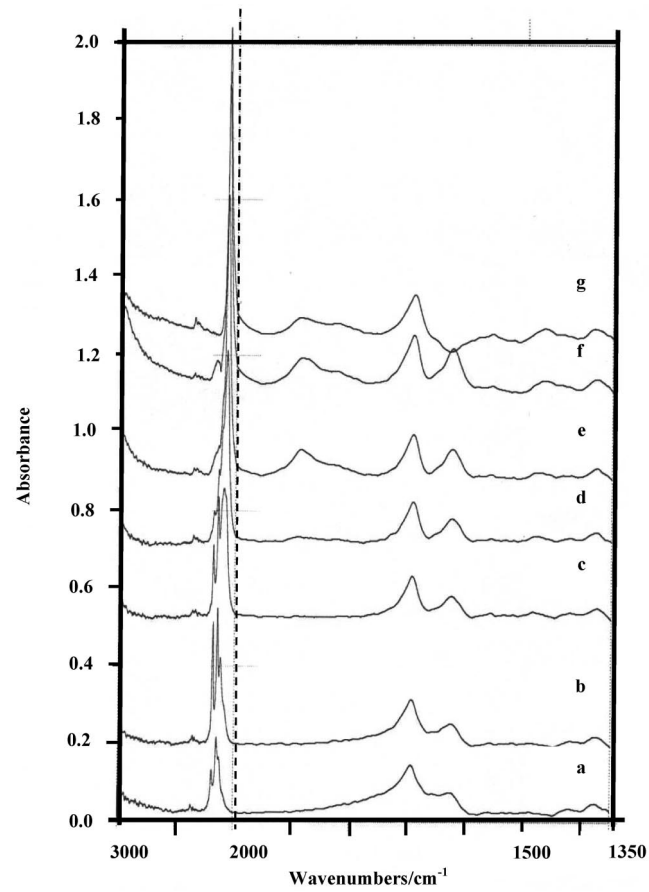

Figure 5. In-situ FTIR spectral changes of Pt nanowires encapsulated in FSM-16 after adsorption of 60 Torr CO and 5 Torr H_2O mixture at 323 K as a function of time. From bottom to top after (a) 3 min, (b) 10 min, (c) 30 min, (d) 50 min, (e) 60 min, (f) evacuation for 15 min, and (g) evacuation for 1 h.

The structure of the formate can be determined by the value of $\delta\nu$ to obey the following order: monodentate formate > free formate > bidentate formate.[31] In the light of this empirical approach, the bands at 1620 and 1370 cm^{-1} might be attributed to a monodentate formate species since the frequency separation (250 cm^{-1}) is higher than that of a free formate ion (220 cm^{-1}).[32]

3.4.2. Pt Particle/FSM-16. Figure 6 shows the spectra recorded after dosing the reacting gas mixture (P_{CO}= 60 Torr and P_{H_2O}= 5 Torr) onto 5 wt% Pt particles/FSM-16, at 323 K, as a function of time. After 3 min of contact time, bands at 2188, 2149, and 1628 cm^{-1} were observed. The subsequent 25 min concurrently led to the appearance of small band at 2128 cm^{-1}, which showed an increase in intensity and a shift to lower wavenumbers (2088 cm^{-1}) together with a band at 1718 cm^{-1}, which noticeably developed with time. The latter absorption band characterizes bond vibration in surface carbonate−carboxylate compounds.[33]

By comparing the bands of Pt particles/FSM-16 with those of Pt wires/FSM-16, one can notice that no characteristic bands for bridge-bonded CO is observed in the IR spectra of the former during the studied reaction time (220 min). The appearance of bands solely assigned to linear CO (2188 and 2149 cm^{-1}) confirms the presence of nonmetallic Pt beside a metallic Pt (2128−2088 cm^{-1}) of lower concentration compared with those on the wire sample. The appreciable increase in intensity of the 1440 cm^{-1} band, ascribed to free carbonate ions,[34] with time at the expense of any intermediate formate species was observed. The carbonate species is considered to arise from CO_2 adsorbed

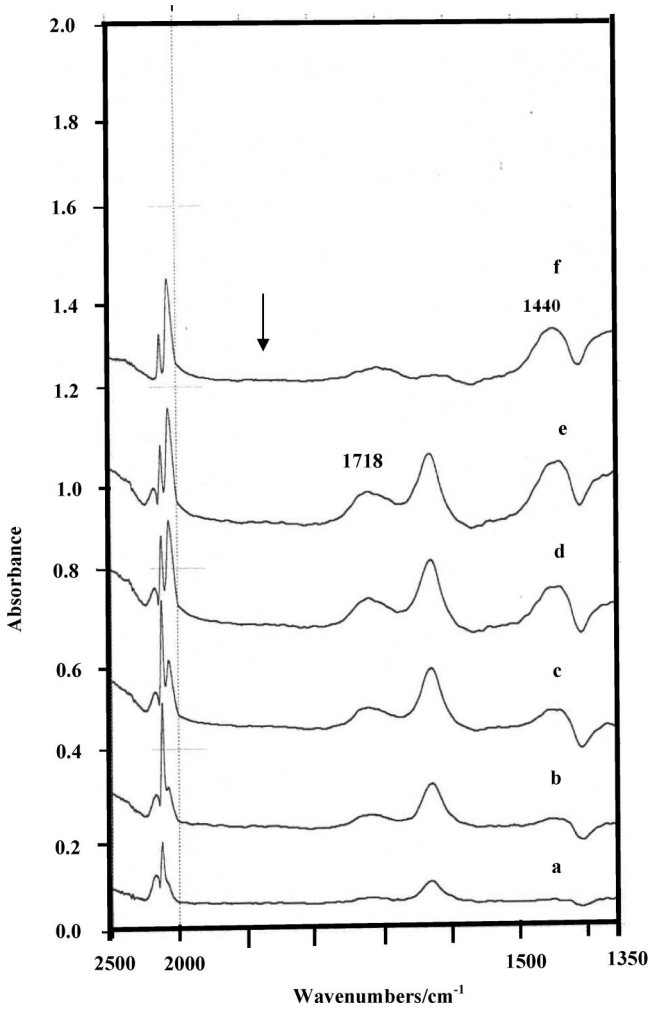

Figure 6. In-situ FTIR spectral changes of Pt nanoparticles encapsulated in FSM-16 after adsorption of a 60 Torr CO and 5 Torr H_2O mixture at 323 K as a function of time. From bottom to top, after (a) 3 min, (b) 25 min, (c) 50 min, (d) 75 min, (e) 100 min, and (f) evacuation till 220 min.

species on the Pt surface; therefore, competitive adsorption on active Pt sites is very much considered in the case of Pt particles. It also seems that the water band at 1628 cm^{-1} is excessively appeared on Pt particles compared with that on the wire. It is worth noting that the 2188 and 2149 cm^{-1} bands tended to disappear very rapidly with time in favor of the metallic carbonyl 2096 cm^{-1} band in the case of Pt wires, whereas they are very reluctant to disappear on Pt particles. This is indicative of the facile reduction of wires compared to particles in enhancing the formation of metallic carbonyl species. The increasing frequency shift of CO-bonded Pt wires (2096 cm^{-1}) compared to that of Pt particles (2088 cm^{-1}) gives a hint on increasing the electron deficiency of Pt wires comparatively.

3.5. Catalytic Performances of WGSR on Pt Wire and Pt Particle/FSM-16. The WGS reaction ($CO + H_2O \rightarrow CO_2 + H_2$) was performed at reduced pressure ($P_{CO} = 60$ Torr, $P_{H_2O} = 5$ Torr) for both samples at 323 K. As shown in Figure 7, Pt wires encapsulated in FSM-16 exhibited higher activity in WGSR (~4 times), forming an equimolar mixture of CO_2 and H_2 than that on Pt particles/FSM-16. An induction period for both catalysts was depicted followed by an abrupt increase in activity with time for the wire sample. On the contrary, a fast deactivation occurred on the Pt particles/FSM-16 sample. It seems that the induction period corresponded ver much to the time necessary for the cluster's formation despite the variation

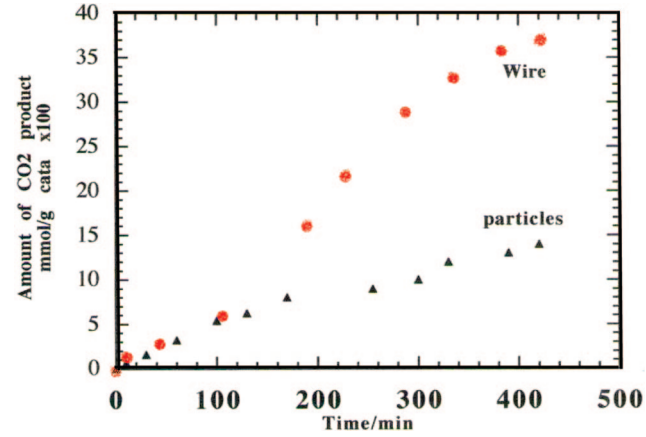

Figure 7. Effect of Pt shape encapsulated in FSM-16 on the activity towards the WGSR at 323 K. Reaction conditions; 5 wt% Pt loading, 0.2 g of catalyst, $P_{CO} = 60$ Torr, $P_{H_2O} = 5$ Torr.

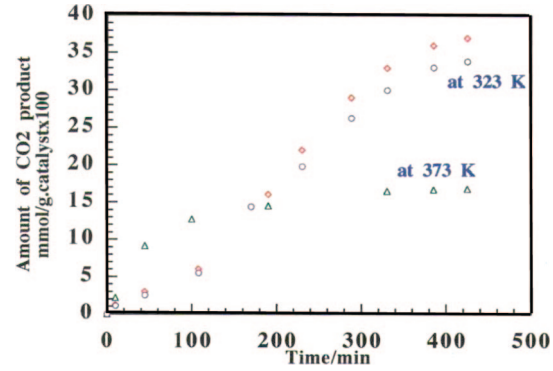

Figure 8. The dependence of the activity (of WGSR) of Pt nanowires on temperatures.

in activity features for both catalysts beyond this period. Performing the same reaction on the wire sample at 323 K (exhausted catalyst) without any treatment maintained almost the same activity, thereby revealing the stability of Pt wires and, most likely, their cohesive energy (Figure 8). This can be explained by the enhancement of nucleophilic attack of H_2O to CO adsorbed on Pt wire/FSM-16, in which the back bonding from Pt to CO is weaker because of the electron deficiency of Pt atoms compared to that of Pt particle/FSM-16, as suggested in TPSR patterns of CO adsorption.

Upon increasing the temperature to 373 K for the wire/FSM-16 sample, a significant drop in activity was obtained (Figure 8). This curve shows no induction period; however, it proceeds quickly, giving a plateau that signifies a deactivation process. It is proposed that this deactivation is supported by the induced increase in metallic Pt^0 nanowires. A fast carbonylation with increasing temperature resulted in an increase in the metallic Pt percentages. This suggests that the high WGS activity is associated with the cationic Pt domains. It can be stated that the strength of the CO cluster bonds depend on the environment of the atom that the CO interact with; thus, the restructuring of wires at 373 K was expected to restrict the Brownian motion of CO along the deformed nanowires.[35]

Discussing the activity of the WGSR in terms of decreasing Pt dispersion (7−9%, Table 1) highlights that this reaction is a structure sensitive (morphology) one. Characterization of Pt/FSM-16 using TPSR, TPR, and FTIR spectroscopy following CO/H_2O adsorption shows that Pt wires acquire electron deficiency on their surface as well as a facile reaction with CO, which together activate the surface reaction of WGS on the Pt

nanowires, comparatively. In addition, Pt metal sites, in the case of wires, provokes the formation of uniformates species, which easily decompose to form CO_2, rather than those of carbonates highly localized and stabilized on Pt particles. The growth of nanowires along the (110) axis might engage them in dissociating CO in a more facile way.[36]

4. Conclusions

FSM-16 encapsulated Pt nanowires and nanoparticles with 5 wt% loading were synthesized, evaluated for WGS reaction, and characterized. Rates for nanowires were significantly higher than those for nanoparticles. Increasing the activity of nanowires was due, in part, to the formation/decomposition of unidentate formate species depicted on its surface where it was counteracted on nanoparticles by existing free carbonates, which is essentially more stable (or surface poisoning) than formates, thus restricting its decomposition into CO_2. It has also been shown that catalytic activity of Pt nanowires depends on the facile binding with CO at lower temperatures than with nanoparticles of well-stabilized and controlled morphology. This study shows that not the specific surface area, for the stabilized nanoparticles, but the geometric structure together with residual cationic Pt largely determines the catalytic performance of nanowires. It has been shown from FTIR results that CO molecules are found to bind at the bridge positions of Pt atoms; as well as on monometallic Pt, on the Pt nanowires where it is restricted only to monometallic Pt; of lower concentration comparatively, on Pt nanoparticles. Binding CO to bridge positions along Pt nanowires facilitates long hopping of CO, random mobility, and thus enabling easy interaction with H_2O.

References and Notes

(1) Saini, R. K.; Chiang, I. W.; Peng, H.; Smalley, R. E.; Billups, W. E.; Hauge, R. H.; Margrave, J. L. *J. Am. Chem. Soc.* **2003**, *125*, 3617.

(2) Hu, J.; Odom, T. W.; Lieber, C. M. *Acc. Chem. Res.* **1999**, *32*, 435.

(3) Sun, S.; Murray, C. B.; Weller, D.; Folks, L.; Moser, A. *Science* **2000**, *287* (5460,), 1989–1992.

(4) Maier, S. A.; Kik, P. G.; Atwater, H. A.; Meltzer, S.; Harel, E.; Koel, B. E.; Requicha, A. A. G. *Nat. Mater.* **2003**, *2*, 229.

(5) Daniel, M.-C.; Astruc, D. *Chem. Rev.* **2004**, *104*, 293.

(6) Mohamed, M. M.; Salama, T. M.; Ohnishi, R.; Ichikawa, M. *Langmuir* **2001**, *17*, 5678.

(7) (a) Schider, G.; Krenn, J. R.; Gotschy, W.; Lamprecht, B.; Ditlbacher, H.; Leitner, A.; Aussengg, F. R. J. *Appl. Phys.* **2001**, *90*, 3825. (b) Mohamed, M. M.; Mekkay, I. J. *Phys. Chem. Solids* **2003**, *64*, 249.

(8) Kitahara, T.; Sugawara, A.; Sano, H.; Mizutani, G. *Appl. Surf. Sci.* **2003**, *219*, 271.

(9) Bae, S. Y.; Seo, H. W.; Park, J.; Yang, H.; Kim, B. *Chem. Phys. Lett.* **2003**, *376*, 445.

(10) Zhang, X. T.; Liu, Z.; Ip, K. M.; Leung, Y. P.; Li, Q.; Hark, S. K. *J. Appl. Phys.* **2004**, *95*, 5752.

(11) Hu, Y.; Gu, H.; Sun, X.; Wang, J.; You, J. *Appl. Phys. Lett.* **2006**, *88*, 193120.

(12) Liu, J.; Duan, J. L.; Toimil-Molares, M. E.; Karim, S.; Cornelius, T. W.; Dobrev, D.; Yao, H. J.; Neumann, R. *Nanotechnology* **2006**, *17*, 1922.

(13) Ohsuna, T.; Terasaki, O.; Hiraga, K. *Mater. Sci. Eng., A* **1996**, *135*, 217–218.

(14) Shin, H. J.; Ryoo, R.; Liu, Z.; Terasaki, O. *J. Am. Chem. Soc.* **2001**, *123*, 1246.

(15) Kumar, S.; Gupta, V.; Sreenivas, K. *Nanotechnology* **2005**, *16*, 1167.

(16) Itaya, K.; Sugawara, S.; Arai, K.; Saito, S. J. *Chem. Eng. Jpn.* **1984**, *17*, 514.

(17) Sun, Y.; Xia, Y. *Science* **2002**, *298*, 2176.

(18) Fukuoka, A.; Higashimoto, N.; Sakamoto, Y.; Inagaki, S.; Fukushima, Y.; Ichikawa, M. *Micro. Meso. Mater.* **2001**, *48*, 171.

(19) Nikoobakht, B.; El-Sayed, M. A. *Langmuir* **2001**, *17*, 6368.

(20) Gao, J.; Bender, C. M.; Murphy, C. J. *Langmuir* **2003**, *19*, 9065.

(21) (a) Yanagisawa, T.; Shimizu, T.; Kuroda, K.; Kato, C. *Bull. Chem. Soc. Jpn.* **1990**, *62*, 763–1535. (b) Inagaki, S.; Fukushima, Y.; Kuroda, K. J. *Chem.Soc., Chem. Commun.* **1993**, 680.

(22) (a) Mohamed, M. M.; Salama, T. M.; Ichikawa, M. J. *Colloid Inter. Sci.* **2000**, *224*, 366. (b) Mohamed, M. M.; Ichikawa, M. J. *Colloid Inter. Sci.* **2000**, *232*, 381.

(23) Fukuoka, A.; Higashimoto, N.; Sakamoto, Y.; Sasaki, M.; Sugimoto, W.; Inagaki, S.; Fukushima, Y.; Ichikawa, M. *Catal. Today* **2001**, *66*, 23.

(24) Mohamed, M. M.; El-Erian, M. A. *Powder Technol.* **1996**, *86*, 239.

(25) Beebe, T. P.; Gelin, P.; Yates, J. T. *Surf. Sci.* **1984**, *148*, 526.

(26) Dell'Amico, D. B.; Calderazzo, F.; Veracini, C. A.; Zandona, N. *Inorg. Chem.* **1984**, *23*, 3030.

(27) D'aniaello, M.J.; Jr.; Carr, C. J.; Zammit, M. G. *Inorg. Synthesis* **1989**, *26*, 319.

(28) Van Santen, R. V.; Rec, T. *Chim. Pays-Bas.* **1982**, *101*, 121.

(29) Kinoshita, K.Carbon., *Electrochemical and Physical Proprties*; Wiley: New York, 1988; p 87.

(30) (a) Grgor'ev, A. I.; Donchenko, N. V.; Dunaeva, K. M.; Debabov, D. V.; Russ, J. *Inorg. Chem.* **1985**, *30*, 497. (b) Mink, J.; Meic; Z.; Gai, M.; Korpar, B.; Colig, J. *Organomet.Chem.* **1983**, *256*, 203.

(31) Mohamed, M. M.; Salama, T. M.; Othman, I.; El-Shobaky, G. A. *Appl. Catal. A* **2005**, *279*, 23.

(32) Meunier, F. C.; Goguet, A.; Hardcre, C.; Burch, R.; Thompsett, D. J. *Catalysis* **2007**, *252* (1), 18.

(33) Nakamoto, K.; *Infrared Spectra of Inorganic and Coordination Compounds (in Russian)*; John Wiley: New York, 1977.

(34) Davydov, A. A. *Infrared Spectroscopy of Adsorbed Species on the Surface of Transition Metal Oxides*; John-Wiley and Sons: 1990; p 38.

(35) Oncel, N.; Van Beek, W. J.; Huijben, J.; Poelsema, B.; Zandvliet, H. J. W. *Surf. Sci.* **2006**, *600* (2), 4690.

(36) McCrea, K.; Parker, J. S.; Chen, P.; Somorjai, G. *Surf. Sci.* **2001**, *494* (3), 238.

JP8009904